

RESEARCH

Open Access



# Environment-Adaptable Fast Multi-Resolution (EAF-MR) optimization in large-scale RF-FPGA systems

Minhee Jun<sup>\*†</sup> , Rohit Negi<sup>†</sup>, Shihui Yin, Mohamed Alawieh, Fa Wang, Megha Sunny, Tamal Mukherjee and Xin Li

## Abstract

Software-defined radio (SDR) can have high communication quality with a reconfigurable RF front-end. One of the main challenges of a reconfigurable RF front-end is finding an optimal configuration among all possible configurations. In order to efficiently find an optimal configuration, Environment-Adaptable Fast (EAF) optimization utilizes calculated signal-to-interference-and-noise ratio (SINR) and narrows down the searching space (Jun et al., Environment-adaptable efficient optimization for programming of reconfigurable Radio Frequency (RF) receivers, 2014). However, we found several limitations for applying the EAF optimization to a realistic large-scale Radio Frequency-Field Programmable Gate Array (RF-FPGA) system. In this paper, we first investigated two estimation issues of RF impairments: a saturation bias of nonlinearity estimates and limited resources for RF impairment estimation. Using the estimated results, the SINR formula was calculated and used for the Environment-Adaptable Fast Multi-Resolution (EAF-MR) optimization, which was designed by applying the EAF optimization to multi-resolution optimization. Finally, our simulation set-up demonstrated the efficiency improvement of the EAF-MR optimization for a large-scale RF-FPGA.

**Keywords:** Software-defined radio (SDR), Reconfigurable RF front-end, Large-scale RF-FPGA, Estimation of RF impairments, Environment-Adaptable Fast Multi-Resolution (EAF-MR) optimization

## 1 Introduction

Wireless communication is ubiquitous in our daily life using an excessive number of communication standards: 3G/4G/LTE cellular service, Wi-Fi, bluetooth, and so on. The new paradigm of Internet of Things (IoT) has also accelerated the plethora of wireless communication [3]. The abundance of communication standards has recently increased interest in cognitive radio because its multi-standard platform supports cost reduction of service suppliers and the efficient use of frequency spectrum.

First, cognitive radio allows for more affordable service to providers and subscribers. Previously, when a new communication standard comes out, service providers have spent a huge amount of expenditure for building a new infrastructure such as base stations and hardware

systems corresponding to a new communication standard. Particularly in rural areas, it is a burdensome and time-consuming process for service suppliers to include rural areas to the new service coverage due to a low user density. However, cognitive radio must have multi-standard platforms in its hardware. Due to the dynamic property of cognitive radio, service providers can reuse the existing infrastructures when serving a new communication standard. Thus, service providers reduce the expensive cost and time for distributing the infrastructure for the new standard.

In addition, cognitive radio is an optimal solution for handling inefficient radio frequency (RF) spectrum utilization. The RF spectrum is a limited natural resource, and it is officially managed by Federal Communications Commission (FCC) [1]. Given the fixed standard assignment policy of government agencies, issues might arise for future wireless communication due to the excessive amount of communication standards. Since the RF spectrum occupation rate has a wide variation, in time and

\*Correspondence: [mjun@ece.cmu.edu](mailto:mjun@ece.cmu.edu)

<sup>†</sup>Equal contributors

Department of Electrical and Computer Engineering, Carnegie Mellon University, Pittsburgh, PA 5000 Forbes Ave, Pittsburgh, 15213 PA, USA

space, from 15 to 85% [1], cognitive radio can dynamically and intelligently change its communication channel and temporally utilize the portions of the unused RF spectrum (called a spectrum hole or white space) [7, 8, 17].

This multi-standard platform of cognitive radio is achieved by implementing software-defined radio (SDR). In order to design the SDR architecture, there have been studies to design fixed wide-band RF front-end. The fixed wide-band RF front-end accommodates various signals on different RF spectrum bands by choosing a homodyne architecture. Also, the fixed wide-band RF front-end generally requires to remove RF filters and to choose durable RF components with wide-band signals [6]. However, the condition of wide-band signals limits the choice of RF components and performance. In contrast, a reconfigurable RF front-end (also called reconfigurable Radio Frequency-Field Programmable Gate Array (RF-FPGA)) is more appropriate for the SDR architecture in terms of selectivity and sensitivity [9].

The reconfigurable RF front-end is a novel RF front-end concept recently proposed by the U.S. Defense Advanced Research Projects Agency (DARPA) [5]. The RF-FPGA replaces with the fixed wideband RF front-end but it is combined with the the classical baseband RF-FPGA [4, 14]. Meanwhile, a reconfigurable RF front-end can be programmed to switch its RF components: there are various RF component banks, including amplifier, filter, and mixer banks as given in Fig. 1 [2, 16]. The details of RF-FPGA architectures are introduced in [12, 13].

This architecture of RF-FPGA as shown in Fig. 1 maximizes the reconfigurability of SDR, and thus, RF-FPGA is an attractive alternative for supporting a multi-standard platform of cognitive radio in the future. Particularly, the enhanced reconfigurability in this RF-FPGA architecture is directly related to increasing the reusability of this device. The RF-FPGA reusability can save

hardware re-design cost for updating wireless communication standards. In addition, RF-FPGA can have a high performance solving the practicality issue of a cognitive radio because it can be dynamically tunable to a particular setting optimized to real-time communication environments in the field.

Note that RF-FPGA operates on RF spectrums, and thus, it is distinguished from digital FPGA that operates on baseband spectrums. It is known that RF-FPGA is beneficial with respect to reduced life cycle cost, reduced re-design cost, and service for multiple DoD platform.

RF-FPGA can dynamically adapt to the communication environment on-the-fly retaining a high communication quality. RF-FPGA is defined as a dynamically reconfigurable (programmable) RF transceiver. RF-FPGA is composed of an array of reconfigurable RF component blocks that can have as many as 100 bits of control. As shown in Fig. 1, the RF component blocks are adjusted by switches that are deployed between the RF component blocks. The switches connect the RF component blocks that are chosen by the reconfiguration engine while bypassing the RF component blocks in the idle mode (i.e., the bypassed RF component blocks are not selected by the reconfiguration engine). This RF-FPGA architecture is designed to maximize the flexibility of RF-FPGA for adapting to varying RF environments. This flexibility of RF-FPGA can allow to change the operating frequency band of the RF transceiver.

A reconfigurable RF front-end can flexibly select one of the RF components arranged in each component bank using switches and serially connect them in different architectures, including heterodyne and homodyne [5]. The ability to have many configurations in component banks supports a multi-standard platform for currently existing standards. The component bank needs to include a number of configurations with different ranges

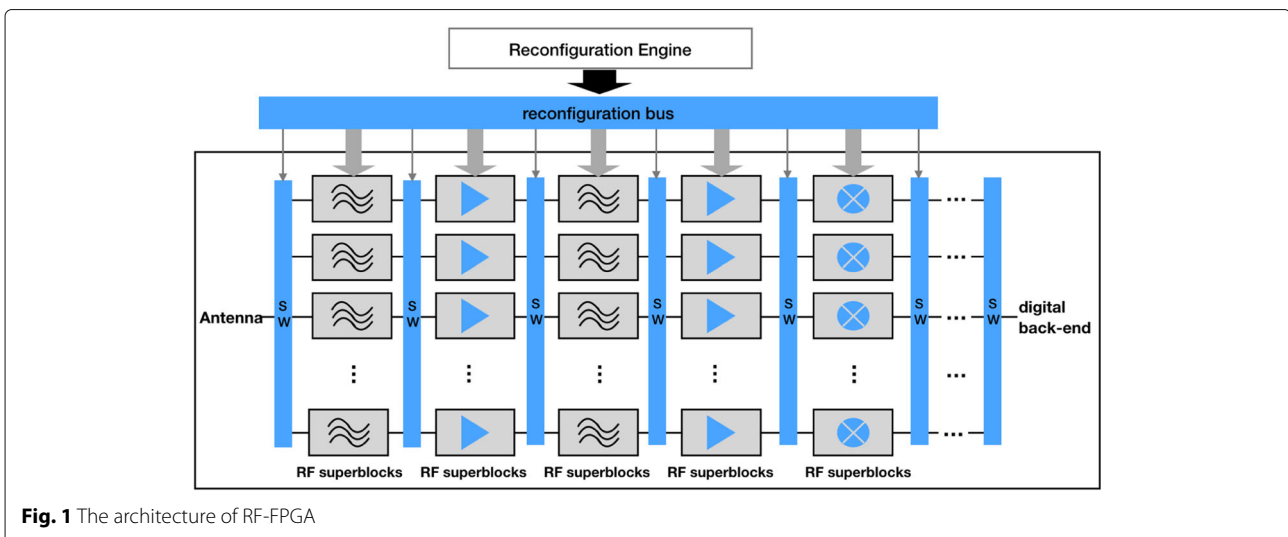


Fig. 1 The architecture of RF-FPGA

to consider future standards. For future standards, the component banks contain many configurations that may not be accounted for current settings. When a reconfigurable RF front-end selects RF components in the component banks, it aims to satisfy the requirements of the given communication standard. Thus, a reconfigurable RF front-end supports a multi-standard platform by dynamically changing its occupying RF spectrum of various standards for cognitive radio.

In order to operate a reconfigurable RF front-end, an important challenge is finding an optimal configuration among all possible configurations (a configuration is mapped to a combination of RF components in a reconfigurable RF front-ends). In order to find the configuration, an optimization problem is defined as finding a configuration that minimizes its cost function (such as power consumption) while satisfying constraint requirements of a given communication standard (such as signal-to-noise ratio (SNR)) [9]. Studies have aimed to solve this optimization problem in a reconfigurable RF front-end. Tao et al.'s study in [15] proposed two-phase relaxation optimization that attempts to reduce the possibility of finding local optimal configurations. This process performs local relaxation optimization in two separate phases: In the first phase, the optimization finds a configuration of the highest SNR; in the second phase, starting from the found configuration, the optimization searches an optimal point using the relaxation optimization. This optimization has improved selectivity of optimal configuration, and thus, when the reconfigurable radio is initially programmed, several base configurations (i.e., default configurations) can be pre-programmed into it, based on the desired communication standards. However, it has a limited capability of reducing reconfiguration load for a dynamic communication environment, with blockers and large interferers appearing randomly at different frequencies. In this case, the reconfigurable RF front-end cannot be pre-programmed exhaustively, since there are too many possible scenarios to be considered. Rather, a fast algorithm to adapt the RF front-end to interferers in real-time is needed. Thus, a fast optimization algorithm—called Environment-Adaptable Fast (EAF) optimization—was proposed for speeding up the optimization of a reconfigurable RF front-end in a dynamic spectrum environment [9].

The EAF optimization improves its optimization efficiency by predicting configurations that are less likely to pass the communication quality requirement of a given standard. The prediction is performed based on signal-to-interference-and-noise ratio (SINR), which is calculated—as opposed to simulated—using RF impairment information. These are three steps of the EAF optimization: (1) RF impairments should be estimated when a reconfigurable RF front-end is manufactured. The estimators

of RF impairments are designed based on the signal model of baseband signals. For RF impairment information, the estimation methods of RF impairments are designed as presented in [9–11]. (2) The SINR calculation formula for the EAF optimization is described in [11]. In the SINR calculation, impairing signal power due to each of the RF impairments—phase noise, IIP3, noise figure—was separately derived in terms of the power of the signal of interest and interference. The SINR calculation uses estimated RF impairments and a signal spectrum in a given communication environment. Thus, real-time blocker information is reflected in SINR calculations. (3) Finally, the EAF optimization uses the SINR calculation to identify the configurations that likely do not meet a SINR specification and to narrow down the search space of configurations. The EAF optimization method was shown to reduce the computational cost significantly, finding an optimal configuration after only five iterations instead of searching all possible configurations exhaustively. Therefore, the EAF optimization method can be successfully utilized as a heuristic to find a minimum power configuration of adequate SNR in an experimental case of a small reconfigurable RF system.

In contrast, a large-scale RF-FPGA poses a significant problem for the EAF optimization. A realistic RF-FPGA is likely to be controlled by several hundred bits that select the component values. In such a large-scale RF-FPGA, it is not possible to directly measure and characterize the RF impairments of each of the possible configurations.

In order to utilize the *large-scale* RF-FPGA for cognitive radio, our research focused on developing an efficient algorithm, called Environment-Adaptable Fast Multi-Resolution (EAF-MR) method. The EAF-MR method has the following contributions:

- (1) *RF impairment estimation in a large-scale RF-FPGA*: we propose a method that estimates unknown RF impairments of the configurations that can not directly estimated using baseband signals in a large-scale RF-FPGA. The configurations with known estimates are used to measure other configurations with unknown RF impairments. This estimation method is useful because only a limited number of configurations in a large-scale RF-FPGA are estimated due to limited time and computation resources.
- (2) *environment-adaptable algorithm*: when choosing an optimal configuration in a large-scale RF-FPGA, the EAR-MR algorithm reflects communication quality changes due to interference in the field. This interference effect is measured using the signal-to-interference-and-noise ratio (SINR) calculation in the algorithm.

- (3) *the improved time-efficiency of EAF-MR optimization algorithm for a large-scale RF-FPGA*: in the EAF-MR algorithm, the EAF optimization synergizes with the multi-resolution method in order to improve the time efficiency of the optimization process in a large-scale RF-FPGA.

In this paper, we investigate a model-based approach to solve this problem in order to use the EAF optimization in large-scale RF-FPGA systems. First, we studied RF impairment estimation for a large-scale RF-FPGA system. We derived statistical signal models of RF impairments, and based on the statistical signal models, we designed estimators of RF impairments. We focused on two main problems while applying the estimators of RF impairments to a large-scale RF-FPGA system: two saturation areas of nonlinearity estimates and limited resources in RF impairment estimation procedures. The saturation areas of nonlinearity estimates are caused by a wide range of RF front-ends. In order to solve the saturation, we designed a formula for changing the transmission signal power in an estimation procedure. Also, we considered limited resources in RF impairment estimation in a large-scale RF front-end. Solving the limited resource problem, we used a design of experiments (DoE) approach that effectively selects sample configurations among the large number of all possible configurations in a large-scale RF-FPGA. We also used an interpolation method that obtains unknown component values from known component values of RF impairments calculated from sample configurations. Second, we derived a formula that calculates SINR in a given communication environment in terms of phase noise, nonlinearity, and noise figure. In order to improve the accuracy of the SINR calculation, the impairing signal power by each RF impairment was separately analyzed considering the frequency offset of interference and the power of the signal of interest and interference. We assumed that RF impairments are estimated, and a signal spectrum is obtained by a signal analyzer [9], a configuration of reconfigurable RF front-ends that bypasses all filters and amplifiers. Third, using the SINR calculation, we designed the EAF-MR optimization method that hastens an optimization process for finding an operable configuration in a large-scale RF-FPGA system. Simulation results showed that our EAF-MR optimization method significantly improves its optimization speed compared with the multi-resolution optimization method.

Now, we clarify the terminologies that will be frequently used in the following context:

- *component*: the element—such as amplifier, filter, or mixer—that composes a reconfigurable RF front-end. The components are placed and switched in RF component banks.
- *configuration*: a cascade of the chosen components from RF component banks in a reconfigurable RF front-end. Configurations can be reconfigured by switching each component.
- *overall RF impairment*: the metric that represents the overall RF impairment of a configuration.
- *component value*: the metric that represents the RF impairment of a component.

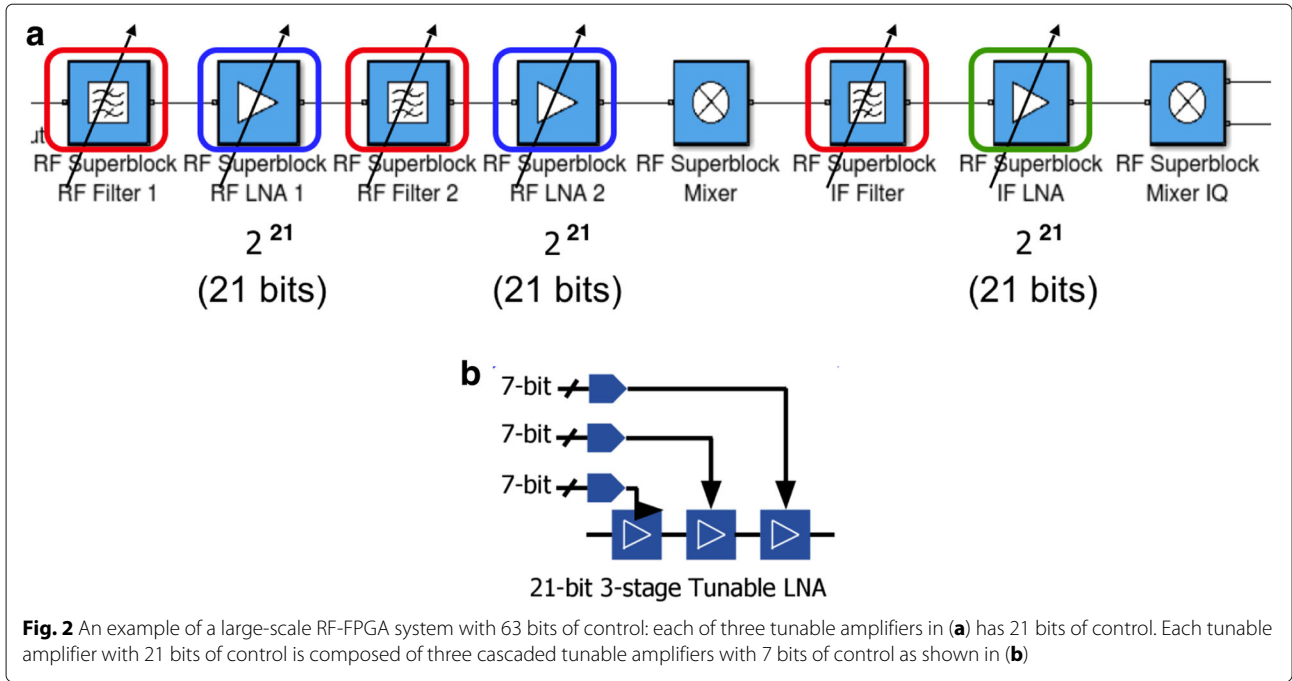
## 2 RF impairment estimation in large-scale RF-FPGA systems

In this section, we investigate the estimation of RF impairments in a *large-scale* RF front-end. RF impairments in a RF system are described in [16], and the basic insight of signal processing is explained in [1, 2, 8, 9]. The first problem associated with this large scale is that the large number of RF front-ends span a wide range of RF impairment values. Due to the wide range of RF impairment values, the RF front-end is very likely to experience saturation in an estimation process when transmission power is fixed. In Section 2.1, we solve this problem by designing a method that adjusts the transmission power during the estimation procedure. The second problem is the large number of configurations in a large-scale RF front-end. This problem is tackled by using a design of experiments (DoE) approach and an interpolation procedure as discussed in Section 2.2. These methods are important in a large-scale RF front-end because we cannot simulate (or estimate) all configurations; we can only simulate a limited number of sample configurations. For example, a reconfigurable RF front-end with 63 bits of control means that the number of configurations is about  $9.2 \times 10^{18}$ , which results in an impractically time-consuming estimation procedure. Our methods of RF impairment estimation in a large-scale RF front-end are utilized to efficiently extract unknown properties of RF components from known properties that are calculated from simulated data. This method of RF impairment estimation is applied to a large-scale RF front-end of 63 bits.

### 2.1 Tackling a wide range of RF impairment values: bias in IIP<sub>3</sub> estimate

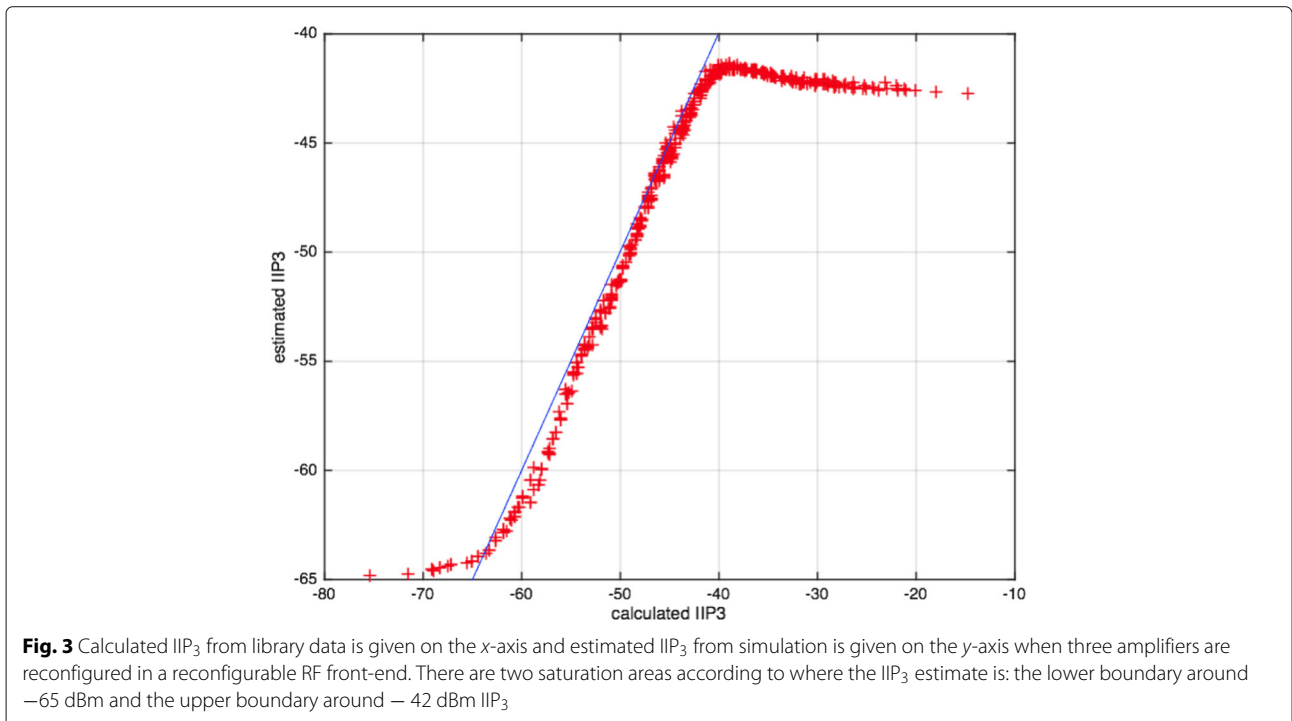
Consider a large-scale RF-FPGA system, as shown in Fig. 2. This example large-scale RF-front-end has three amplifiers with 21 bits of control. This front-end has 63 bits of control, allowing a wide range of values for gain and the third-order input intercept points (IIP<sub>3</sub>). This is defined in terms of the ratio of the first order gain over the third order gain. Due to this, configurations with a wide range of IIP<sub>3</sub> values are possible.

Figure 3 shows that the wide range of IIP<sub>3</sub> results in bias in estimated IIP<sub>3</sub>. Specifically, we found two areas of large bias: lower boundary around  $-65$  dBm and upper boundary around  $-43$  dBm. The wide range within the



estimated  $IIP_3$  from  $-80$  to  $-10$  dBm is mainly due to high gains obtained by passing through multiple amplifiers. In order to solve the bias (saturation) problem in  $IIP_3$  estimation, we obtained a formula for adjusting transmission power to a RF front-end. The transmission power  $P_{tx}$  was derived from the upper and lower boundaries of  $IIP_3$  saturation.

The upper boundary of  $IIP_3$  saturation is related to thermal noise. Thermal noise power should be smaller than the intermodulated signal power of transmitted signals in order to be detected during the estimation procedure. More specifically, the overall thermal noise power after passing a reconfigurable RF front is given as  $NF_{0(dBm/Hz)} + \Delta f_{(dB)} + NF_{(dB)}$  where thermal noise floor is  $NF_0$  (dBm/Hz) =



$-174(\text{dBm}/\text{Hz})$ ,  $\Delta f_{(\text{dB})} = 10 \cdot \log_{10} B_{(\text{dB})}$  for the bandwidth  $B_{(\text{Hz})}$  of the transmitted signal, and  $NF_{(\text{dB})}$  is an additional noise figure for noise margin. Meanwhile, the intermodulated signal with  $\text{IIP}_3$  has a power of  $3 \cdot P_{\text{sig}(\text{dBm})} - 2 \cdot \text{IIP}_3(\text{dBm})$  where  $P_{\text{sig}}$  is the nominal transmitted signal power of the two transmitted signals that are intermodulated. So, we derive the following condition to allow accurate estimation of  $\text{IIP}_3$ .

$$NF_0(\text{dBm}/\text{Hz}) + \Delta f_{(\text{dB})} + NF_{(\text{dB})} < 3 \cdot P_{\text{sig}(\text{dBm})} - 2 \cdot \text{IIP}_3(\text{dBm}), \quad (1)$$

where  $\Delta f_{(\text{dB})} = 10 \cdot \log_{10} B_{(\text{dB})}$ .

From this, the upper boundary of  $\text{IIP}_3$  saturation is given as,

$$\begin{aligned} \text{IIP}_3(\text{dBm}) &< \frac{1}{2} (3 \cdot P_{\text{sig}(\text{dBm})} - (NF_0(\text{dBm}/\text{Hz}) + \Delta f_{(\text{dB})} + NF_{(\text{dB})})) \\ &= P_{\text{sig}(\text{dBm})} + \frac{1}{2} (P_{\text{sig}(\text{dBm})} - (NF_0(\text{dBm}/\text{Hz}) + \Delta f_{(\text{dB})} + NF_{(\text{dB})})). \end{aligned} \quad (2)$$

The lower boundary of  $\text{IIP}_3$  saturation in Fig. 3 is related to the transmitted signal power  $P_{\text{sig}}$ . A transmitted signal with a high power level suffers from nonlinearity intermodulation. When an intermodulated signal by the third order nonlinearity has a power as large as the power of a transmitted sinusoid, the transmission power is defined as  $\text{IIP}_3$ . Thus, the transmitted signal power  $P_{\text{sig}}$  should be smaller than  $\text{IIP}_3$  as follows,

$$P_{\text{sig}(\text{dBm})} < \text{IIP}_3(\text{dBm}). \quad (3)$$

From (2) and (3), the range of  $\text{IIP}_3$  over which we can expect low bias is given as,

$$K_0 < \text{IIP}_3(\text{dBm}) < K_0 + \Delta K, \quad (4)$$

where  $K_0 = P_{\text{sig}(\text{dBm})}$  and  $\Delta K = \frac{1}{2} (P_{\text{sig}(\text{dBm})} - (NF_0(\text{dBm}/\text{Hz}) + \Delta f_{(\text{dB})} + NF_{(\text{dB})}))$ .

Now, we specify the choice of transmission power  $P_{\text{tx}(\text{dBm})} = P_{\text{sig}(\text{dBm})} + \Delta P_{(\text{dB})}$  that should be used for  $\text{IIP}_3$  estimation to allow low bias.

The overall  $\text{IIP}_3$  of a configuration of cascaded components is as follows,

$$\frac{1}{\text{IIP}_3} = \frac{1}{\text{IIP}_{3,1}} + \frac{G_1}{\text{IIP}_{3,2}} + \dots + \frac{G_1 \cdot G_2 \cdot \dots \cdot G_{N-1}}{\text{IIP}_{3,N}}, \quad (5)$$

where  $\text{IIP}_{3,k}$ ,  $G_k$ , are the  $\text{IIP}_3$  and gain of the  $k$ th component for  $k = 1, 2, \dots, N$ .

From this, we can assume that the nonlinearity of the last cascaded component is dominant, i.e.,  $\frac{1}{\text{IIP}_3} \approx \frac{G_1 \cdot G_2 \cdot \dots \cdot G_{N-1}}{\text{IIP}_{3,N}}$ . In that case,  $\text{IIP}_3$  is given as

$$\text{IIP}_{3(\text{dBm})} \approx \text{IIP}_{3,N(\text{dBm})} - G_1^{N-1}(\text{dB}) \text{ where } G_1^{N-1} \text{ is the overall gain of the first } N-1 \text{ components: } G_1^{N-1}(\text{dB}) = G_{1(\text{dB})} + G_{2(\text{dB})} + \dots + G_{N-1}(\text{dB}).$$

Thus, (4) is given as in terms of the  $\text{IIP}_3$  of the last component,

$$K_0 + G_1^{N-1}(\text{dB}) < \text{IIP}_{3,N(\text{dBm})} < K_0 + \Delta K + G_1^{N-1}(\text{dB}). \quad (6)$$

Now, we assume that the approximate range of  $\text{IIP}_3$  such as  $\text{IIP}_{3,N}^{(\text{min})}$  and  $\text{IIP}_{3,N}^{(\text{max})}$  of (the last) component is known. We define the transmission power increase  $\Delta P$  over the nominal value  $P_{\text{sig}(\text{dBm})}$  for use in  $\text{IIP}_3$  estimation. Then, the range of power increase  $\Delta P$  that satisfies (6) is given as follows,

$$\begin{aligned} \Delta P^{(\text{max})}(\text{dB}) &= \text{IIP}_{3,N}^{(\text{min})}(\text{dBm}) - (K_0 + G_1^{N-1}(\text{dB})) \\ \Delta P^{(\text{min})}(\text{dB}) &= \text{IIP}_{3,N}^{(\text{max})}(\text{dBm}) - (K_0 + \Delta K + G_1^{N-1}(\text{dB})). \end{aligned} \quad (7)$$

Thus, we choose  $\Delta P$  to be the mean of  $\Delta P^{(\text{max})}(\text{dB})$  and  $\Delta P^{(\text{min})}(\text{dB})$  in order to avoid  $\text{IIP}_3$  estimation saturation.

$$\begin{aligned} \Delta P_{(\text{dB})} &= \text{mean} \left( \Delta P^{(\text{max})}(\text{dB}), \Delta P^{(\text{min})}(\text{dB}) \right) \\ &= 0.5 \cdot \left( \text{IIP}_{3,N}^{(\text{min})}(\text{dBm}) + \text{IIP}_{3,N}^{(\text{max})}(\text{dBm}) \right) \\ &\quad - K_0 - 0.5 \cdot \Delta K - G_1^{N-1}(\text{dB}). \end{aligned} \quad (8)$$

Thus, in a large-scale RF front-end, the transmission power  $P_{\text{tx}}$  for  $\text{IIP}_3$  estimation is given as,

$$\begin{aligned} P_{\text{tx}(\text{dBm})} &= P_{\text{sig}(\text{dBm})} + \Delta P_{(\text{dB})} \\ &= 0.5 \cdot (\text{IIP}_{3,N}^{(\text{min})}(\text{dBm}) + \text{IIP}_{3,N}^{(\text{max})}(\text{dBm})) \\ &\quad - 0.5 \cdot \Delta K - G_1^{N-1}(\text{dB}). \end{aligned} \quad (9)$$

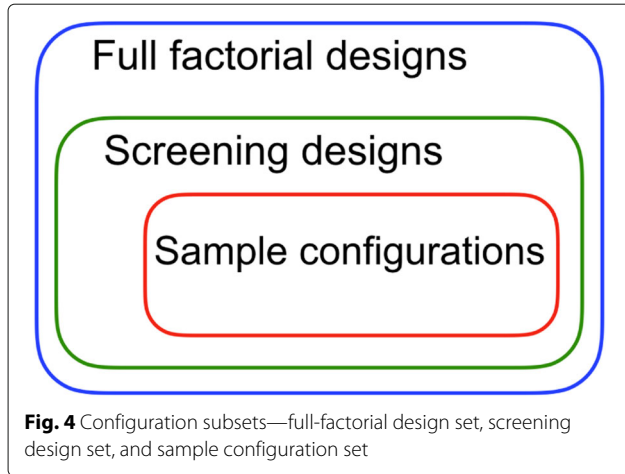
## 2.2 Tackling a large number of configurations: DoE and interpolation methods

A significant challenge in applying the EAF optimization method to a large-scale RF front-end is that RF impairment estimation is time-consuming when the number of configurations is very large. In this section, we use model-based design of experiments (DoE) and interpolation methods to drastically reduce the time needed for estimation.

### 2.2.1 Configuration subsets: full-factorial design set, screening design set, and sample configuration set

The configurations of a large-scale RF front-end can be successively narrowed into the following subsets: full-factorial design set, screening design set, and sample configuration set as shown in Fig. 4.

First, a *full-factorial design set* includes all possible configurations for a large-scale RF front-end. In our example in Fig. 2, assuming three fixed filters and three reconfigurable amplifiers with 21 bits of control that are composed of three 7-bit sub-amplifiers, the set of full-factorial design has configurations with 63 bits of control. A *screening*



*design set* is a subset of the full-factorial design set and includes the most significant factors of configurations. The configurations of a screening design set are obtained by reconfiguring only a few of the most significant bits (MSBs) of sub-amplifiers as seen in Fig. 5. In our example, two MSBs of three sub-amplifiers are allowed to be reconfigured with the remaining bits held constant at 0, resulting in a screening design set of configurations with 18 bits of control. Finally, *sample configurations* are selected for actual simulation and data collection from within the screening design set.

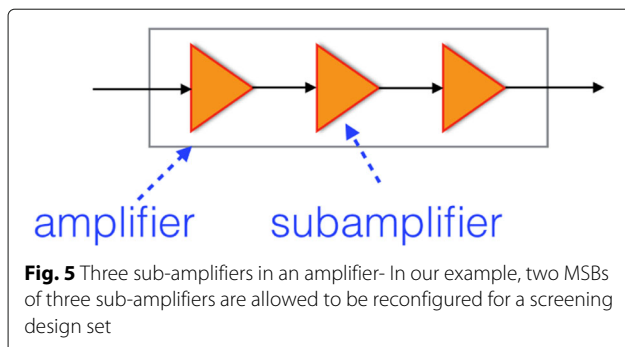
**2.2.2 Configuration subsets and RF impairment calculation**

In a cascaded chain of RF components, as in Fig. 2, we can calculate the overall RF impairment from the component values using the following formula,

$$G^A_{(dB)} = G_{1(dB)} + G_{2(dB)} + \dots + G_{N(dB)}, \tag{10}$$

$$\frac{1}{IIP_{3^A}} = \frac{1}{IIP_{3,1}} + \frac{G_1}{IIP_{3,2}} + \dots + \frac{G_1 \cdot G_2 \cdot \dots \cdot G_{N-1}}{IIP_{3,N}}, \tag{11}$$

$$F^A - 1 = F_1 - 1 + \frac{F_2 - 1}{G_1} + \frac{F_3 - 1}{G_1 \cdot G_2} + \dots + \frac{F_N - 1}{G_1 \cdot G_2 \cdot \dots \cdot G_{N-1}}, \tag{12}$$



where  $G_k$ ,  $IIP_{3,k}$ , and  $F_k$  are the gain,  $IIP_3$ , and noise factor, respectively, of the  $k$ th component of a configuration ( $k = 1, 2, \dots, N$ ), and  $G^A$ ,  $IIP_{3^A}$ , and  $F^A$  are the overall gain,  $IIP_3$ , and noise factor, respectively, of the configuration.

Thus, in order to obtain an unknown value of overall RF impairments, we need to obtain the component values of RF impairments. We will now explain how to obtain component values from sample configurations and how to select sample configurations based on a linear model of RF components in Section 2.2.3.

**2.2.3 Linear model of RF impairments in a large-scale RF-FPGA**

We note that, perhaps surprisingly, (10), (11), and (12) are all of the same general linear form,

$$Z = h_1 X_1 + h_2 X_2 + \dots + h_k X_k + \dots + h_N X_N, \tag{13}$$

where  $X_k$  represents the RF impairment of the  $k$ th component of a configuration,  $h_k$  is a coefficient for the  $k$ th term,  $k = 1, 2, \dots, N$ , and  $Z$  represents the overall RF impairment of the configuration. The impairment can be either gain ( $X_k = G_{k(dB)}$ ),  $IIP_3$  ( $X_k = 1/IIP_3$ ), or noise factor ( $X_k = F_k - 1$ ). For example, for (11),  $X_k = \frac{1}{IIP_{3,k}}$ ,  $h_1 = 1$ ,  $h_k = G_1 \cdot G_2 \cdot \dots \cdot G_{k-1}$ , for  $k \in \{2, \dots, N\}$ .

When the value of the  $k$ th component  $X_k$  is chosen in a set of component values,  $\{\theta_{k,1}, \theta_{k,2}, \dots, \theta_{k,C_k}\}$ , we can define the vector  $\theta$  that is composed of all available component values as follows,

$$\theta = \left[ \underbrace{\theta_{1,1}, \theta_{1,2}, \dots, \theta_{1,C_1}}_{\theta_{1,C_1}}, \underbrace{\theta_{2,1}, \theta_{2,2}, \dots, \theta_{2,C_2}}_{\theta_{2,C_2}}, \dots, \underbrace{\theta_{N,1}, \theta_{N,2}, \dots, \theta_{N,C_N}}_{\theta_{N,C_N}} \right]^T. \tag{14}$$

Then, we can build a linear model,

$$Y = H \cdot \theta + N, \tag{15}$$

where  $Y$  is the vector of measured RF impairment using simulation or actual measurement (each element corresponding to one sample configuration that is simulated) while the vector  $N$  represents measurement noise during the estimation process.

We will now present how to define the matrix  $H$  in (15). The  $k$ th component  $X_k$  in (13) chooses a component value  $\theta_{k,k'}$  in (14) ( $k' \in \{1, 2, 3, \dots, C_k\}$ ), and (13) is given as follows,

$$\begin{aligned} Y &= h_1 \theta_{1,1'} + h_2 \theta_{2,2'} + \dots + h_k \theta_{k,k'} + \dots + h_N \theta_{N,N'} + N \\ &= [h_1 \cdot \mathbf{g}_1, h_2 \cdot \mathbf{g}_2, \dots, h_k \cdot \mathbf{g}_k, \dots, h_N \cdot \mathbf{g}_N] \cdot \theta \\ &= \mathbf{h}' \cdot \theta \end{aligned} \tag{16}$$

where the row sub-vector  $\mathbf{g}_k$  in  $\mathbf{h}'$  is defined as follows,

$$(\mathbf{g}_k)_{1,l} = \begin{cases} 1 & \text{if } l = k' \\ 0 & \text{otherwise,} \end{cases} \quad (17)$$

where  $l = 1, 2, 3, \dots, C_k$ .

Thus, we can define the matrix  $\mathbf{H}$  in (15) composed of the row vector  $\mathbf{h}'$  in (16) corresponding to the measured sample configuration  $Y$ .

Based on (15), we obtain the unknown characteristics  $\hat{\theta}$  of all components using least-squares (LS) estimation as below,

$$\hat{\theta} = (\mathbf{H}^T \cdot \mathbf{H})^{-1} \cdot \mathbf{H} \cdot \hat{\mathbf{Y}}. \quad (18)$$

Given any configurations with unknown RF impairment, we can use (13) to estimate its impairment using the estimated component values  $\hat{\theta}$ . Thus, using a screening design set of sample configurations, we can estimate component values  $\hat{\theta}$  and use the method (13) to predict the RF impairments of any configurations as shown in Fig. 6.

### 2.2.4 DoE for choosing optimal sample configurations

We select a set of *optimal* sample configurations among the configurations in the screening design set using the design of experiments (DoE) approach. The DoE method selects an optimal set of  $m$  sample configurations (equivalently, the matrix  $\mathbf{H}$  in (18) corresponding to the  $m$  selected sample configurations) using a D-optimal design approach. In the matrix  $\mathbf{H}$ , each row corresponds to one of sample configurations. The D-optimal design approach iteratively updates a set of sample configurations in order to increase the determinant  $|\mathbf{H}^T \cdot \mathbf{H}|$ , i.e., minimize the log-determinant of noise variance matrix in (15) to find optimal sample configurations. The matrix  $\mathbf{H}$  is updated until its conditional number—the ratio of the maximal eigenvalue of  $\mathbf{H}$  over the minimal eigenvalue of  $\mathbf{H}$ —is small. The condition of a small conditional number prevents an error in  $\mathbf{Y}$  from causing a large error in  $\theta$  in 15

The implementation details of the DoE method for choosing sample configurations are described in Algorithm 1 (Appendix).

### 2.2.5 Simulation results

Figure 7 shows the simulation results of gain and IIP<sub>3</sub> estimation by applying the DoE method to the RF-FPGA (Fig. 2). We verify that the method can be successfully used to estimate RF impairments of any configuration using a model-based approach, with component values estimated by a DoE method.

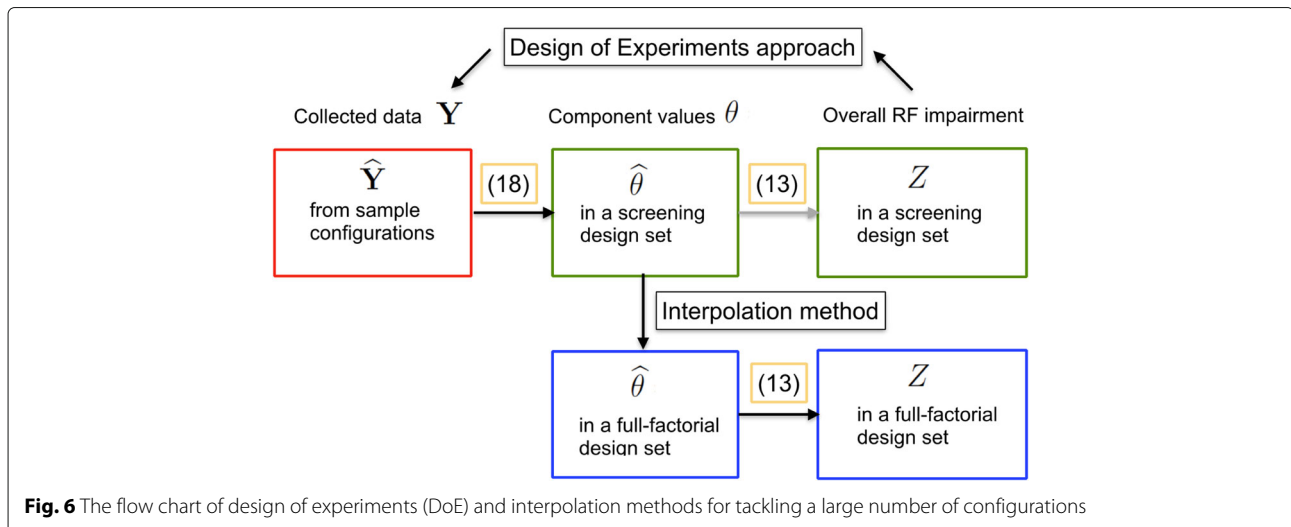
The estimated gain and IIP<sub>3</sub>,  $\hat{Y}$  in (18), of sample configurations are plotted on the  $y$ -axis against true gain and IIP<sub>3</sub>  $Y$  of the sample configurations on the  $x$ -axis in Fig. 7a and b respectively. The simulation results show that the estimates of  $\hat{Y}$  proportionally increase with true values of  $Y$ . (At high gain values, around 100 dB, the estimates begin to saturate in Fig. 7a. Also, configurations where at least one amplifier is bypassed have IIP<sub>3</sub> estimates which are about 3 dB lower in Fig. 7b.)

The estimated gain and IIP<sub>3</sub>,  $\hat{\theta}$  of the three amplifiers, are plotted on the  $y$ -axis against true gain and IIP<sub>3</sub>  $\theta$  of the three amplifiers on the  $x$ -axis in Fig. 7c and d respectively. The estimates  $\hat{\theta}$  proportionally increase with true values of  $\theta$ . (The estimated IIP<sub>3</sub> of the first and second amplifiers are about 3 dB lower than that of the third amplifier in Fig. 7d.)

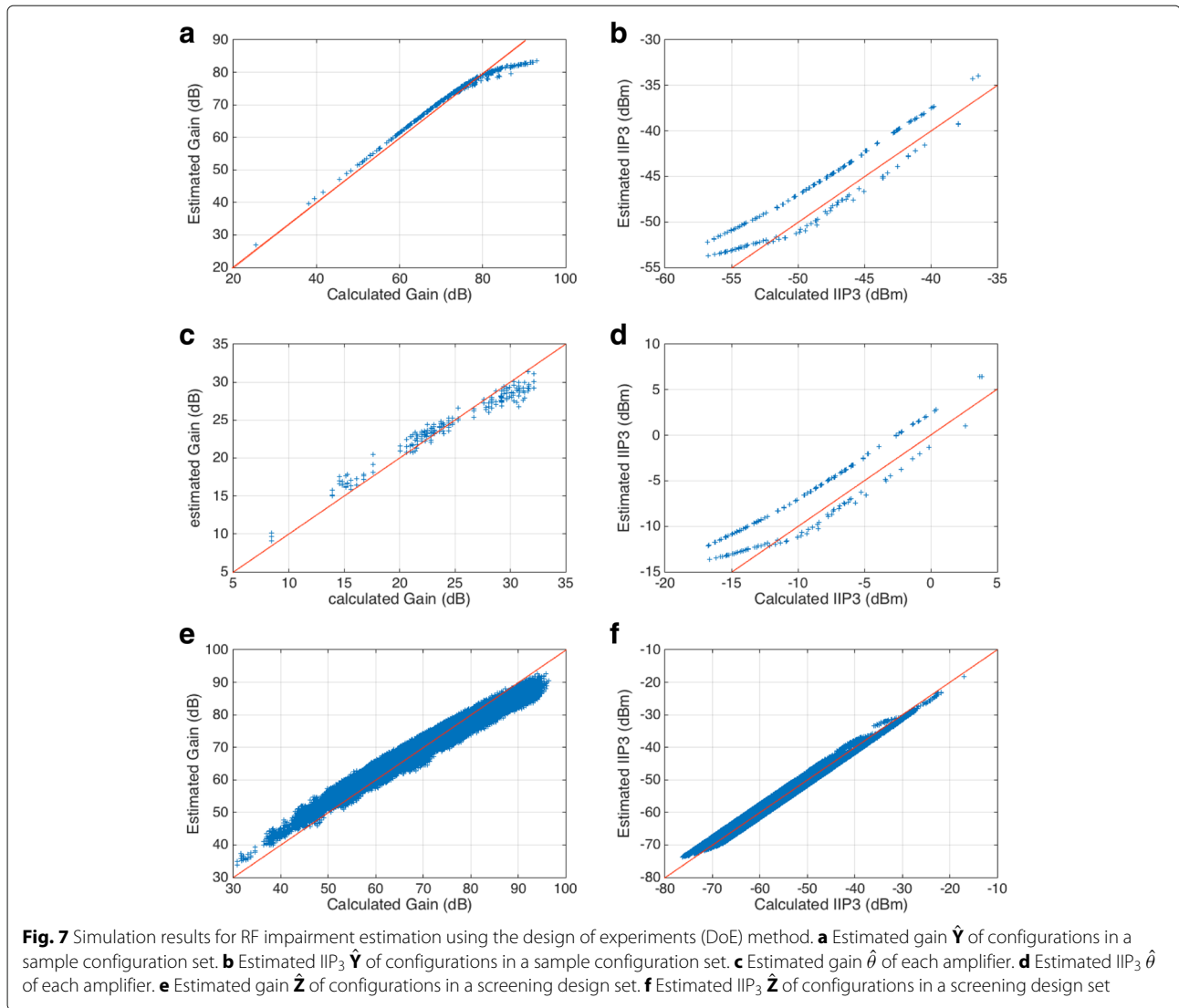
Finally, the estimated gain and IIP<sub>3</sub>,  $\hat{Z}$ , of the remaining configurations in the screening design set are plotted on the  $y$ -axis against true gain and IIP<sub>3</sub>  $Z$  on the  $x$ -axis in Fig. 7e and f respectively. The estimates  $\hat{Z}$  proportionally increase with true values of  $Z$ .

### 2.2.6 Interpolation method

In order to extend the RF impairments estimated for configurations in the screening design set to the full-factorial







design set, the interpolation method is applied. Recollect that the configurations in the screening design set only use a few of the most significant bit (MSB) bits of each component, with the other bits frozen to zero. The assumption made here is that the bits of each component define a real number (or set of real numbers) and that the true RF impairment is a continuous function of this (set of) real numbers.

The red data points shown in Fig. 8—the configurations in a screening design set—have identified values  $\hat{\theta}$  in (18) obtained from the sample configurations as described in Section 2.2.4. The stared points—the configurations in a full factorial design set—have unknown but identifiable values by applying the interpolation method. First, the parameters in a mathematical model are determined to fit data of configurations in a screening design set to the mathematical model. Second, using the parameters

and the mathematical model, the interpolation method interpolates the unknown component values in configurations. The pseudocode of the interpolation method is given in Algorithm 2. For the interpolation process, we utilized the natural neighbor interpolation. Simulation results of applying the interpolation method are plotted in Fig. 9. Thus, we could measure configurations in a full-factorial design set from a screening design set.

The gain and IIP<sub>3</sub> characteristics of amplifiers in the full-factorial design set on the y-axis are obtained by applying the interpolation method to the corresponding estimators of the screening design set. Figure 9a, b, which shows gain and IIP<sub>3</sub> respectively on the y-axis, shows close agreement with the true values on the x-axis.

The obtained RF impairment estimates using the interpolation method are applied to calculate the overall RF impairments of the configurations in the full-factorial set

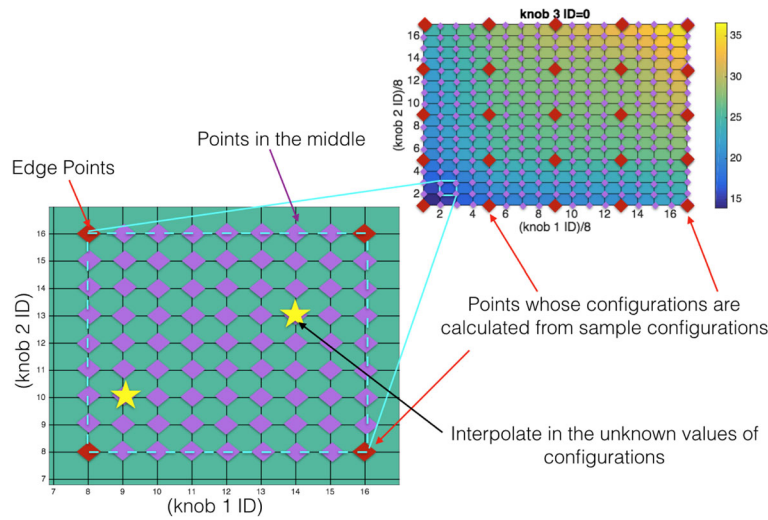


**Fig. 8** The interpolation method is applied to obtain information of the configurations with known RF impairments from the configurations with unknown RF impairments

using the formula (10), (11), and (12). The calculated overall gain and IIP<sub>3</sub> of 150 configurations in a full factorial set on the *y*-axis are plotted against the true values on the *x*-axis in Fig. 9c, d respectively while estimates of gain and IIP<sub>3</sub> obtained by simulation of the same configurations representing a full-factorial set are plotted in Fig. 9e, f. The results demonstrate that unknown RF impairments of the configurations in a full factorial design set are successfully obtained by applying the interpolation method.

**2.2.7 Efficiency of the design of RF impairment estimation for a large-scale RF-FPGA**

In this section, we discuss how the design of RF impairment estimation for a large-scale RF-FPGA improves the efficiency of RF impairment estimation. The designed DoE and interpolation methods are applied to measure RF impairment in a large-scale RF front-end of 63 bits from sample configuration data. In Table 1, the number of simulations (runs) and the required estimation time are calculated for three configuration sets: a full-factorial design set, a screen designing set (of reconfiguring two MSBs of knobs), and a sample configuration set. The simulation time required for the estimation of gain is 41 s while IIP<sub>3</sub> is 42 s. The number of configurations to be simulated is about 10<sup>19</sup>, 2.6 × 10<sup>5</sup>, and 384 in a full-factorial design set, a screening design set, and a sample configuration set, respectively. The total required simulation time is about 1.3 × 10<sup>13</sup> years, 3 × 10<sup>3</sup> h, and 4.4 h, respectively. We found that while estimating RF impairments for a full-factorial or screening design set is costly and time-consuming, estimating RF impairments for sample configurations are powerful and cost-effective, as shown in the Table 1. Thus, we verify that the design

of RF impairment estimation for a large-scale RF-FPGA is important to utilize limited resources, such as time and power, for estimation.

**3 SINR calculation in a large-scale RF-FPGA**

The signal-to-interference-and-noise ratio (SINR) of a configuration is calculated as described in [11] and given as below,

$$SINR = \frac{P_s}{P_{phn} + P_{ip3} + P_n}, \tag{19}$$

**Table 1** Comparison of time consumption for RF impairment estimation

RF impairments	Gain	IIP <sub>3</sub>
Simulation running time for a configuration	41 s	42 s
The number of simulations for full-factorial designs	10 <sup>19</sup> runs	10 <sup>19</sup> runs
The number of simulations for screening designs (2 MSBs of components are reconfigured)	2.6 × 10 <sup>5</sup> runs	2.6 × 10 <sup>5</sup> runs
The number of simulations for sample configurations	384 runs	384 runs
Total simulation time for full factorial designs	1.3 × 10 <sup>13</sup> years	1.33 × 10 <sup>13</sup> years
Total simulation time for screening designs	3 × 10 <sup>3</sup> h	3.1 × 10 <sup>3</sup> h
Total simulation time for sample configurations	4.37 h	4.45 h

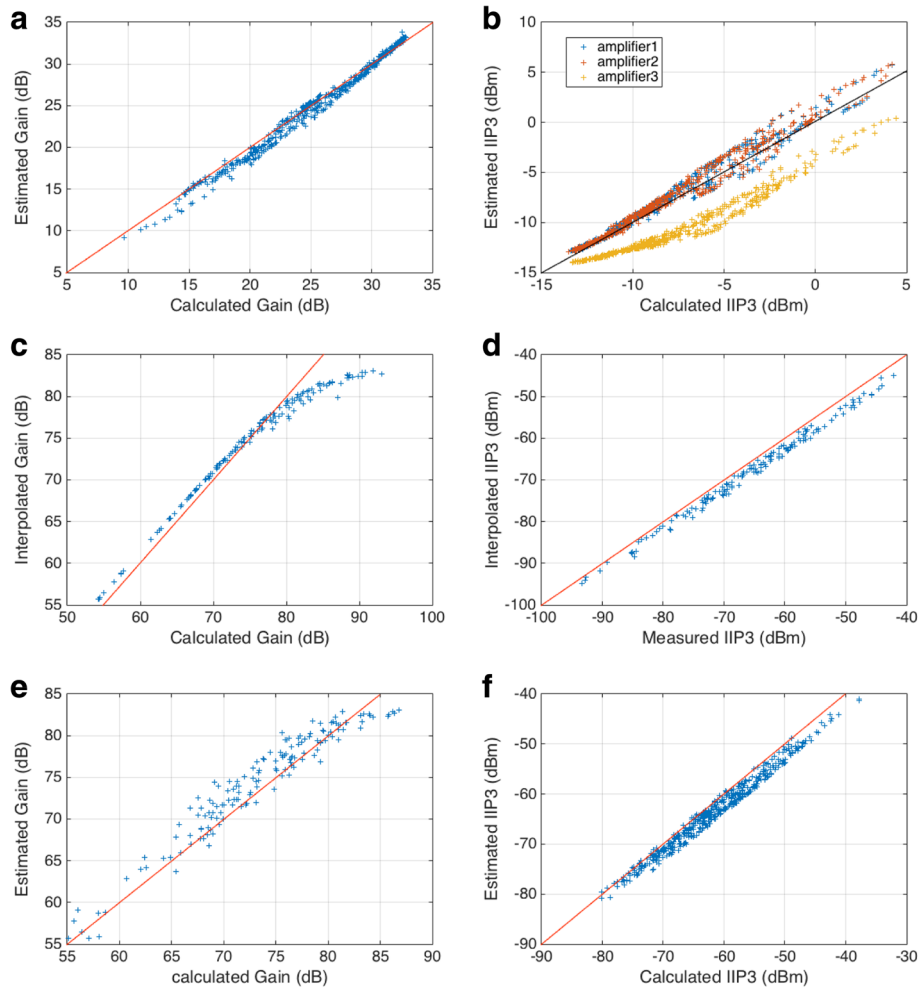


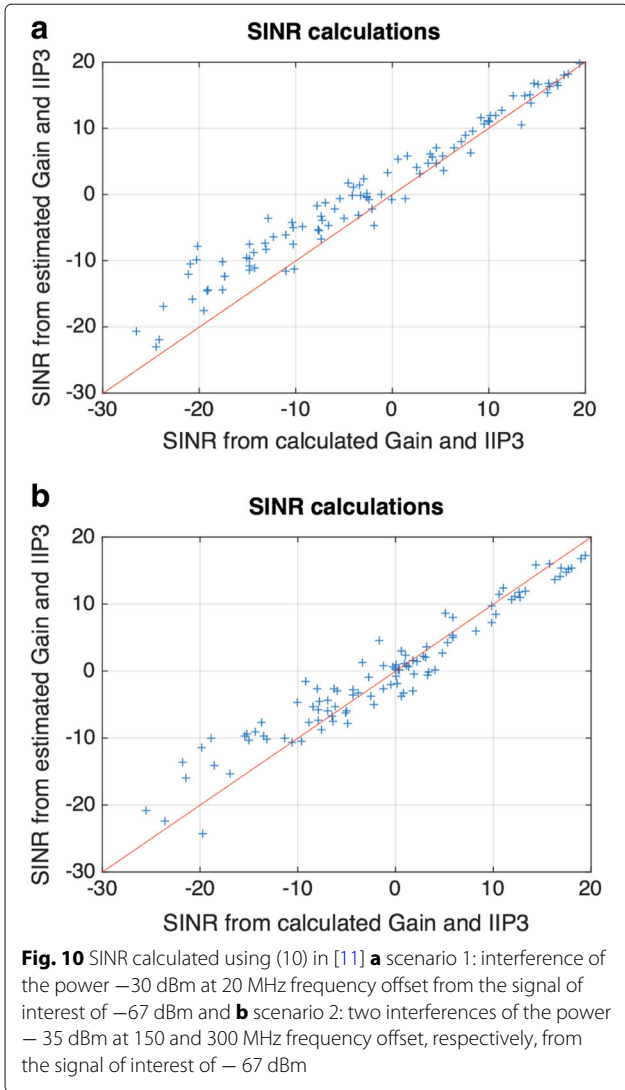
**Fig. 9** Simulation results of the interpolation method. **a** Interpolated gain of an amplifier. **b** Interpolated IIP<sub>3</sub> of an amplifier. **c** Estimated gain of a configuration with three amplifiers using interpolated gain. **d** Estimated IIP<sub>3</sub> of a configuration with three amplifiers using interpolated IIP<sub>3</sub>. **e** Estimated gain of a configuration using simulation. **f** Estimated IIP<sub>3</sub> of a configuration using simulation

where  $P_S$  is the signal power,  $P_{phn}$ ,  $P_{ip3}$ , and  $P_n$  are the impairing signal powers caused by phase noise impairment, nonlinearity impairment, and thermal noise impairment, respectively.

For the SINR calculation in a large-scale RF front-end, we combined the previous estimation methods of RF impairments for obtaining  $P_{phn}$  and  $P_{ip3}$  and our new approach to extend the estimation methods to a large-scale RF front-end. The  $P_{phn}$  and  $P_{ip3}$  in the SINR calculation can be calculated from the estimation methods of RF impairments introduced in [9–11]. Using the estimation methods, the parameters of RF impairments were directly obtainable for all available configurations of a small-scale reconfigurable RF front-end. However, the designed methods cannot be utilized in a large-scale reconfigurable RF front-end due to the limitation of time resource as discussed in Section 4.3. Thus, for the SINR

calculation in a large-scale reconfigurable RF front-end, we use the estimated RF impairments obtained by applying the DoE approach and the interpolation method. The details of the designed estimation method of RF impairments for a large-scale reconfigurable RF front-end were introduced in Section 2.2.

To compare the SINR calculation that uses estimated RF impairments to the SINR calculation using true component values, we considered two scenarios: (1) interference of the power  $-30$  dBm at 20 MHz frequency offset from the signal of interest of  $-67$  dBm and (2) two interferences of the power  $-35$  dBm at 150 and 300 MHz frequency offset, respectively, from the signal of interest of  $-67$  dBm. Figure 10 shows that the SINR calculated by using estimated values of RF impairments is in the reasonable range of the SINR calculated by using true values of RF impairments.



#### 4 EAF-MR optimization in a large-scale RF-FPGA

##### 4.1 Optimization problem in a large-scale RF-FPGA

The optimization problem for searching an optimal configuration in a *small-scale* reconfigurable RF front-end was previously defined in [9–11] as follows,

$$\begin{aligned} \min \quad & F(\mathbf{x}), \\ \text{s.t.} \quad & g_k(\mathbf{x}) \geq G_k \text{ for } 1 \leq k \leq K \end{aligned} \quad (20)$$

where the vector-valued  $\mathbf{x}$  indicates one of the available configurations for a reconfigurable RF front-end, and each element of  $\mathbf{x}$  represents the parameter value of an individual component.  $F(\mathbf{x})$  is a cost function such as power consumption of  $\mathbf{x}$ , which needs to be minimized, while  $g_k(\mathbf{x}) \geq G_k$  ( $1 \leq k \leq K$ ) describe constraints such as SINR.

However, this optimization model in (20) is not suitable to describe the optimization problem in a *large-scale* reconfigurable RF front-end due to the explosively

increased size of search space. With the increased search space in a large-scale reconfigurable RF front-end, the limited time resource causes a bottleneck for a practical use of the previously suggested optimization methods. Practically, the amount of time consumed to obtain SINR using simulation (or measurement) in an optimization process dramatically increases in a large-scale reconfigurable RF front-end. Thus, one of the important factors to be considered in a large-scale reconfigurable RF front-end is reducing the number of simulations (or measurements) for obtaining SINR in an optimization process.

Including this search space factor (e.g., the number of simulations), we now define the optimization problem in a large-scale reconfigurable RF front-end with a new cost function  $F(\mathbf{x}) + H(n)$  as follows,

$$\begin{aligned} \min \quad & F(\mathbf{x}) + H(n), \\ \text{s.t.} \quad & g_k(\mathbf{x}) \geq G_k \text{ for } 1 \leq k \leq K \end{aligned} \quad (21)$$

where  $H(n)$  is a function of the suggested total number  $n$  of simulations (or measurements) in a given optimization algorithm. In our example of a large-scale RF front-end with 63 bits of control, the optimization problem in (21) is given by defining that  $F(\mathbf{x})$  is the power consumption of the configuration  $\mathbf{x}$ ,  $g_1(\mathbf{x})$  is the SINR of  $\mathbf{x}$ ,  $G_1$  is the SNR threshold of the given communication standard,  $K = 1$ , and  $H(n)$  is given as  $\log_2(n)$ .

We note that according to the choice of optimization algorithms, an optimal configuration  $\hat{\mathbf{x}}$  that satisfies the optimization problem in (21) can vary because there is a trade of the costs  $F(\mathbf{x})$  and  $H(n)$ . If a designed algorithm runs more iterations of algorithms to find an optimal configuration, the cost of  $F(\mathbf{x})$  decreases but the cost  $H(n)$  increases, and vice versa. Thus, the optimal configurations of different optimization algorithms may not be the same according to how to design the algorithms.

Solving the defined optimization problem, we introduce the Environment-Adaptable Fast Multi-Resolution (EAF-MR) optimization designed for a large-scale RF-FPGA to adapt to the dynamic conditions in communication.

##### 4.2 EAF-MR optimization

We designed the EAF-MR optimization method [9] by applying the EAF optimization that utilizes the SINR calculation to the multi-resolution optimization.

The multi-resolution optimization primarily has a similar structure as the two-phase relaxation optimization [15]. In the first phase, the multi-resolution optimization iteratively finds the configuration of maximal SINR. In the second phase, starting from the found configuration, the multi-resolution optimization finds an optimal configuration that has the lowest power consumption satisfying the SNR specification for a given communication standard.

The multi-resolution optimization improve the two-phase relaxation optimization for a large-scale reconfigurable RF front-end. The multi-resolution optimization narrows down the search space into screening design sets of available configurations in a large-scale RF front-end. The size of screening design sets is determined by the number of active reconfiguration knob bits in all RF components. The fewer active bits of knobs, the more sparsely the characteristic values of the configurations in the screening design sets are distributed. The multi-resolution optimization tries to search for two types of configurations in the two phases, from small to large active bits. If there is no improvement for one cycle of iterations for all configurations, the iterative reconfiguration is stopped. The pseudocode of the multi-resolution algorithm is given in Algorithm 3 (Appendix).

In our EAF-MR optimization method, we applied the primary algorithmic structure of the multi-resolution optimization, and we utilized the calculated SINR in order to reduce the number of configurations to be simulated. When the SINR calculation of the configurations does not meet the pre-defined SINR threshold, the configurations are trimmed out in the list of configurations to be simulated. The pseudocode of the multi-resolution algorithm is given in Algorithm 4 (Appendix).

### 4.3 Search space of optimization methods

In numerical experiments, we focus only on the multi-resolution optimization and the EAF-MR optimization instead of including traditional optimization methods: exhaustive search, simulated annealing search, local relaxation search (the details of these traditional optimization methods are described in [9]). However, the necessary search space for configurations in a large-scale RF front-end is too big to include these traditional optimization algorithms in Table 2. Assume that a large-scale RF front-end has  $K$  reconfigurable(tuable) components, and its  $k$ th component has the  $l$ th component values of  $N(k, l)$  bits where  $l \in \{1, 2, \dots, C_k\}$  and  $k \in \{1, 2, \dots, K\}$ . The search space of exhaustive search is given as  $O(\prod_k \prod_l 2^{N(k, l)}) = O(2^{\sum_k \sum_l N(k, l)})$ . Simulated annealing search also has a search space of  $O(2^{\sum_k \sum_l N(k, l)})$ . Local relaxation search has a search space of  $O(\sum_k 2^{\sum_l N(k, l)})$ . Multi-resolution search has a search space of  $O(\sum_k \sum_l 2^{N(k, l)})$ . For example, there are  $K = 3$  amplifiers that has  $C_k = 3$  sub-amplifiers with  $N(k, l) = 7$  bits of control in Fig. 5. In this example, the number of simulations per one iteration of exhaustive search, simulated annealing search, local relaxation search, and multi-resolution search are  $9.22 \times 10^{18}$ ,  $\approx 9.22 \times 10^{18}$ ,  $O(6.29 \times 10^6)$ , and  $O(1.15 \times 10^3)$ , respectively (during this one iteration a series of cascaded components

**Table 2** Search space of optimization methods

Optimization method	Search space	No. simulations per iteration when $K = 3, C_k = 3, N(k, l) = 7$
Exhaustive search	$O(2^{\sum_l \sum_k N(k, l)})$	$2^{3 \times 3 \times 7} = 2^{63} = 9.22 \times 10^{18}$
Simulated annealing search	$O(2^{\sum_l \sum_k N(k, l)})$	$\leq 9.22 \times 10^{18}$
Local relaxation search	$O(\sum_k 2^{\sum_l N(k, l)})$	$3 \times 2^{3 \times 7} = 6.29 \times 10^6$
EAF optimization	$O(\sum_k 2^{\sum_l N(k, l)})$	$\leq 3 \times 2^{3 \times 7} = 6.29 \times 10^6$
Multi-resolution search	$O(\sum_k \sum_l 2^{N(k, l)})$	$1.15 \times 10^3$
EAF-MR optimization	$O(\sum_k \sum_l 2^{N(k, l)})$	$\leq 1.15 \times 10^3$

in a large-scale RF front-end is reconfigured only once).

The EAF optimization and the EAF-MR optimization have the same search space as the local relaxation and the multi-resolution search, respectively. However, these optimization methods reduce the search spaces by eliminating candidate configurations that have SINR calculation under a threshold. The size of reduced search space depends on the communication environment in a field.

Reducing search space is a critical factor in the optimization of a large-scale RF front-end due to practical time consumption. For this reason, it is impractical to apply classical methods to a large-scale RF front-end. However, the search space is dramatically reduced from exponential increase in exhaustive search to linear increase in multi-resolution search in terms of the number of configurations and the number of components as shown in Table 2. Therefore, multi-resolution search and the EAF-MR optimization method are practically applicable in a large-scale RF front-end.

Table 3 shows the upper bounds of  $H(n)$  in (21) assuming  $C_k$  and  $N(k, l)$  are given as  $L$  and  $N_0$  respectively. We can observe that the upper bound of  $H(n)$  is significantly reduced in multi-resolution search and the EAF-MR optimization in terms of the base 2 logarithms. Also, Table 3 shows an example case of  $H(n)$  after one iteration when  $K = 3$ ,  $C_k = 3$ , and  $N(k, l) = 7$ . The observed values prove that multi-resolution search and the EAF-MR optimization significantly reduce  $H(n)$  in (21) from 63 to 10.17. It demonstrates that the two optimization methods are the most efficient to minimize the cost function  $F(\mathbf{x}) + H(n)$  presented in (21). Thus, in order to search the optimal configuration of reconfigurable RF front-end when solving the optimization problem in (21), multi-resolution and the EAF-MR optimization are the algorithms of our interest, and thus are focused in simulation.

In the next section, we are going to show simulation results of multi-resolution search and the EAF-MR optimization.

**Table 3**  $H(n)$  in (21) of optimization methods

Optimization method	$H(n)$ after $M$ iteration assuming $C_k = L$ and $N(k, l) = N_0$	$H(n)$ after one iteration ( $M = 1$ ), when $K = 3$ , $C_k = 3$ and $N(k, l) = 7$
Exhaustive search	$L \cdot K \cdot N_0 + \log_2 M$	63
Simulated annealing search	$\leq L \cdot K \cdot N_0 + \log_2 M$	$\leq 63$
Local relaxation search	$L \cdot N_0 + \log_2 K + \log_2 M$	33.28
EAF optimization	$\leq L \cdot N_0 + \log_2 K + \log_2 M$	$\leq 33.28$
Multi-resolution search	$N_0 + \log_2 L + \log_2 K + \log_2 M$	10.17
EAF-MR optimization	$\leq N_0 + \log_2 L + \log_2 K + \log_2 M$	$\leq 10.17$

#### 4.4 Simulation

We finally demonstrate the performance of our EAF-MR optimization using a Matlab simulation.

##### 4.4.1 Simulation setting

We verified the performance of the designed EAF-MR optimization in a large-scale RF-FPGA (Fig. 2) using Matlab Simulink. In the simulation, we used the communication standard IEEE 802.11g, and the required SNR specification is 11.5 dB. The transmitted signals have the bandwidth 20 MHz and the power  $-67$  dBm. The RF-FPGA has 63 bits, which implies approximately  $10^{19}$  configurations. There are two fixed RF filters, one fixed IF filter, and three 21 bit amplifiers. The power consumption range of all possible configurations is from 11.85 to 107.85 mW. We tested two optimization methods, multi-resolution and EAF-MR, on the scenario, which has one interferer of  $-30$  dBm at 20 MHz frequency offset from the signal of interest.

##### 4.4.2 Simulation results

Tables 4 and 5 show the simulation results of the multi-resolution search and the EAF-MR optimization. While the multi-resolution optimization method took 2172 simulations for finding an optimal configuration, our EAF-MR optimization method required only two simulations. The EAF-MR optimization increases optimization efficiency since it is able to discard a large number of configurations whose calculated SINR does not satisfy the SNR specification. As shown in Table 5, multi-resolution search took 816 and 1356 simulations in phase 1 and phase 2, respectively, whereas the MR-EAF optimization needed 1 and 1 simulation in phase 1 and phase 2, respectively.

Both optimization methods found optimal configurations that satisfy the SNR specification (11.5 dB) as shown in Table 5. In terms of power consumption, we found that

**Table 4** Simulation results of no. simulations

Optimization	Phase I	Phase II	Total number method of simulations
Multi-resolution optimization	816	1356	2172
MR-EAF optimization	1	1	2

there is a trade-off between higher power consumption and the number of simulations. The power consumption of the EAF-MR's optimal configuration is around 21 mW compared to around 12 mW (multi-resolution's optimal configuration). The power consumption of the EAF-MR's optimal configuration is almost twice of that of multi-resolution search. However, the maximal power consumption of all possible configurations is larger than 100 mW. Compared to the maximal power consumption, the EAF-MR optimization found an optimal configuration that has a power consumption in a reasonable range of energy efficiency.

The simulation results verify that our EAF-MR optimization method is appropriately designed for a large-scale reconfigurable RF front-end to perform fast reconfiguration in dynamic communication environments. Table 6 shows that the cost function of the MR-EAF optimization in the optimization problem (21) is significantly improved compared to that of the multi-resolution search. Although the two optimization methods give two different optimal configurations, the cost function in (21) is dropped with the MR-EAF optimization because it needs only a few reconfigurations to find the optimal one.

## 5 Conclusion

In this paper, we investigated the application of the EAF optimization in a large-scale RF-FPGA. To estimate RF impairments in a large-scale RF front-end, we solved two main problems. First, we solved the saturation of non-linear estimates due to a wide range of RF front-ends. To avoid the saturation problem, we obtained a formula for adjusting transmission power for an estimation procedure. Second, we solved a limited estimation resources problem. Because of a large number of configurations, it is not possible to directly measure and characterize the RF impairments of all possible configurations. We extended the estimation procedure to a large-scale RF-FPGA using the design of experiments (DoE) approach and the interpolation method. Finally, we designed an

**Table 5** Simulation results of optimization

Optimization method	Power (mW)	SINR (dB)	Total number of simulations
Multi-resolution optimization	12.52	11.63	2172
MR-EAF optimization	20.98	15.55	2

**Table 6** Simulation results and cost function in the optimization problem (21)

Optimization method	$F(\mathbf{x})$	$H(n)$	$F(\mathbf{x}) + H(n)$
Multi-resolution optimization	12.52	11.08	33.60
MR-EAF optimization	20.98	1	21.98

EAF multi-resolution (EAF-MR) optimization method in which the EAF optimization method was applied to a multi-resolution (MR) optimization. Simulation results showed that our EAF-MR optimization requires only two iterations while multi-resolution optimization takes more than 2000 iterations. There is a trade-off between efficiency and local optimum. However, as an optimal configuration exists, finding a global optimum is not necessary. The main focus of our research is attaining low computational cost (fast convergence) in optimization for a real-time application. Therefore, using this algorithm, reconfigurable RF front-ends can move forward to a reliable multi-standard platform for the needs of future communication systems.

In the future, we want to investigate spectral strategies that help to prune the space of RF configurations to be explored (“search space”) and rules to automatically rank preferred RF configurations. In order to narrow down the search space, we plan to study the heuristic rules that are applicable using the reconfigurability of filters and local oscillators (LOs). While reconfiguring filters and LOs, we assume that the characteristics of RF components (e.g., filters’ center frequency and bandwidth) and also the signal spectrum are accessible. When a blocker appears, in order to improve communication quality, in addition to the choice of filters, etc., we can also change either radio frequency (RF) or intermediate frequency (IF) of the RF system based on the blocker information in the signal spectrum. For example, the blocker signal can be effectively eliminated if it is placed on the stopband of a notch filter in the frequency domain. In order to satisfy this condition, the IF of a reconfigurable RF front-end can be changed by reconfiguring LOs considering the characteristics of the notch filter. The heuristic strategies for reconfiguring filters and LOs will help a reconfigurable RF front-end improve the speed of an optimization process in dynamic communication environments.

## Appendix

In line 1,  $m$  is the number of sample configurations to be selected from a screening design set given in the matrix  $\mathbf{X}_{\text{Screening}}$  in order to estimate RF impairments.  $\mathbf{X}_{\text{Screening}}$  is a row matrix composed of all configurations in a screening design set that is obtained by reconfiguring a few pre-defined MSBs of sub-amplifiers. In line 3,  $\mathbf{H}_{\text{Screening}}$  is

**Algorithm 1** The DoE Approach: find  $\mathbf{X}_{\text{DoE}}$  (a set of sample configurations) and a matrix  $\mathbf{H}_{\text{DoE}}$  in (15).

---

```

1: INPUT:  $m, \mathbf{X}_{\text{Screening}}$ 
2:  $N_{\text{condition}} = \infty$  ▷ conditional number
3: while  $N_{\text{condition}} > N_{\text{condition}}^{(\text{threshold})}$  do
4:    $\mathbf{X}_{\text{DoE}} = \text{function}_{\text{d-optimal method}}(m, \mathbf{H}_{\text{Screening}})$ 
5:    $\mathbf{H}_{\text{DoE}} = \text{function}_{\text{amplifier ID to H}}(\mathbf{X}_{\text{DoE}})$ 
6:    $\lambda^{(\text{max})} \leftarrow$  the maximum of eigenvalues of  $\mathbf{H}_{\text{DoE}}^T \cdot$ 
      $\mathbf{H}_{\text{DoE}}$ 
7:    $\lambda^{(\text{min})} \leftarrow$  the minimum of eigenvalues of  $\mathbf{H}_{\text{DoE}}^T \cdot$ 
      $\mathbf{H}_{\text{DoE}}$ 
8:    $N_{\text{condition}} = \lambda^{(\text{max})} / \lambda^{(\text{min})}$ 
9: end while
10: OUTPUT:  $\mathbf{X}_{\text{DoE}}, \mathbf{H}_{\text{DoE}}$ 

```

---

the matrix  $\mathbf{H}$  in (15) corresponding to  $\mathbf{X}_{\text{Screening}}$ . In line 3,  $N_{\text{condition}}^{(\text{threshold})}$  is a constant of the maximal limit of condition number  $N_{\text{condition}}$ .

In line 1,  $\mathbf{X}_{\text{test}}$ ,  $\mathbf{X}_{\text{known}}$ , and  $\mathbf{V}_{\text{known}}$  are a matrix that indicates a set of test configurations, a set of configurations with known component values, and a set of the known component values in  $\mathbf{X}_{\text{known}}$ , respectively. In the for-loop, the values  $\mathbf{v}_{\text{test}}$  of each component  $\mathbf{x}_{\text{test}}$  are interpolated on the  $i$ th component—separately in the cascaded order—of configurations  $\mathbf{V}_{\text{test}}$ .  $\mathbf{v}_{\text{known}}$  corresponds to  $\theta$  in (14), and  $\mathbf{x}_{\text{known}}$  has the indices of the known component values in a full-factorial set. The interpolation is performed based on the known component values  $\mathbf{v}_{\text{known}}$  and  $\mathbf{x}_{\text{known}}$  using natural neighbor interpolation.

In Algorithm 3,  $\mathbf{x}^{(\text{current})}$ ,  $\text{SNR}^{(\text{current})}$ ,  $\text{Power}^{(\text{current})}$  represent a current configuration, the simulated SNR, and power of the current configuration, respectively.  $n\text{Bit}_1$

**Algorithm 2** The Interpolation Approach: estimate unknown component values  $\mathbf{V}_{\text{test}}$  for test configurations  $\mathbf{V}_{\text{test}}$  in a full factorial set.

---

```

1: INPUT:  $\mathbf{X}_{\text{test}}, \mathbf{X}_{\text{known}}, \mathbf{V}_{\text{known}}$ 
2:  $N \leftarrow$  the number of components in the configurations of  $\mathbf{X}_{\text{test}}$ 
3: for  $i = 1, 2, 3, \dots, N$  do
4:    $\mathbf{x}_{\text{known}} \leftarrow$  the  $i$ -th cascaded component of a configuration of  $\mathbf{X}_{\text{known}}$ 
5:    $\mathbf{x}_{\text{test}} \leftarrow$  the  $i$ -th cascaded component of the configurations of  $\mathbf{X}_{\text{test}}$ 
6:    $\mathbf{v}_{\text{known}} \leftarrow$  component values corresponding to  $\mathbf{X}_p$ . it is obtainable from  $\mathbf{V}_{\text{known}}$ 
7:    $\mathbf{v}_{\text{test}} \leftarrow \text{function}_{\text{interpolation}}(\mathbf{x}_{\text{known}}, \mathbf{v}_{\text{known}}, \mathbf{x}_{\text{test}})$ 
8:    $\mathbf{V}_{\text{test}}(i) \leftarrow \mathbf{v}_{\text{test}}$ 
9: end for
10: OUTPUT:  $\mathbf{V}_{\text{test}}$ 

```

---

**Algorithm 3** Multi-Resolution Algorithm

---

```

1: INPUT: nBit1, nBit2
2:  $\mathbf{x}^{(current)} \leftarrow \mathbf{x}^{(initial)}, \text{SNR}^{(current)} \leftarrow \text{SNR}^{(initial)}, \text{Power}^{(current)} \leftarrow \text{Power}^{(initial)}$ 
3: for  $n = 1, 2, \dots, \text{nBit}_1$  do
4:    $\mathbf{c} \leftarrow$  the initial component of  $\mathbf{x}^{(current)}$ 
5:   while (there has been recent updates on  $\mathbf{x}^{(current)}$ ) do
6:      $\mathbf{c} \leftarrow$  the next available component of the current component  $\mathbf{c}$ 
7:      $\mathbf{X} \leftarrow$  a set of configurations obtained by reconfiguring the component  $\mathbf{c}$  with  $n$  bits of control while other components are fixed.
8:      $\text{SNR}(\mathbf{x}) \leftarrow$  simulated (or measured) SNR for  $\forall \mathbf{x} \in \mathbf{X}$ 
9:      $\text{Power}(\mathbf{x}) \leftarrow$  power for  $\forall \mathbf{x} \in \mathbf{X}$ 
10:     $\mathbf{x}^{(max)} \leftarrow \arg \max_{\mathbf{x} \in \mathbf{X}} \text{SNR}(\mathbf{x})$ 
11:     $\text{SNR}^{(max)} \leftarrow \text{SNR}(\mathbf{x}^{(max)})$ 
12:    if  $\text{SNR}^{(max)} > \text{SNR}^{(current)}$  then
13:       $\mathbf{x}^{(current)} \leftarrow \mathbf{x}^{(max)}, \text{SNR}^{(current)} \leftarrow \text{SNR}^{(max)}$ 
14:       $\text{Power}^{(current)} \leftarrow \text{Power}(\mathbf{x}^{(current)})$ 
15:    end if
16:  end while
17: end for
18: for  $n = 1, 2, \dots, \text{nBit}_2$  do
19:    $\mathbf{c} \leftarrow \mathbf{c}^{(initial)}$ 
20:   while (there has been recent updates on  $\mathbf{x}^{(current)}$ ) do
21:      $\mathbf{c} \leftarrow$  the next available component of the current component  $\mathbf{c}$ 
22:      $\mathbf{X} \leftarrow$  a set of configurations obtained by reconfiguring the component  $\mathbf{c}$  with  $n$  bits of control while other components are fixed.
23:      $\text{SNR}(\mathbf{x}) \leftarrow$  simulated (or measured) SNR for  $\forall \mathbf{x} \in \mathbf{X}$ 
24:     if ( $\mathbf{c}$  is a component in a filter) then
25:        $\mathbf{x}^{(max)} \leftarrow \arg \max_{\mathbf{x} \in \mathbf{X}} \text{SNR}(\mathbf{x})$ 
26:        $\text{SNR}^{(max)} \leftarrow \text{SNR}(\mathbf{x}^{(max)})$ 
27:       if  $\text{SNR}^{(max)} > \text{SNR}^{(current)}$  then
28:          $\mathbf{x}^{(current)} \leftarrow \mathbf{x}^{(max)}, \text{SNR}^{(current)} \leftarrow \text{SNR}^{(max)}, \text{Power}^{(current)} \leftarrow \text{Power}(\mathbf{x}^{(current)})$ 
29:       end if
30:     else if ( $\mathbf{c}$  is a component in an amplifier) then
31:        $\mathbf{x}^{(current)} \leftarrow \arg \min_{\mathbf{x} \in \mathbf{X}, \text{s.t. } \text{SNR}(\mathbf{x}) \geq \text{SNR}_{\text{Spec}}} \text{Power}(\mathbf{x})$ 
32:        $\text{SNR}^{(current)} \leftarrow \text{SNR}(\mathbf{x}^{(current)}), \text{Power}^{(current)} \leftarrow \text{Power}(\mathbf{x}^{(current)})$ 
33:     end if
34:   end while
35: end for
36: OUTPUT:  $\mathbf{x}^{(current)}, \text{SNR}^{(current)}, \text{Power}^{(current)}$ 

```

---

**Algorithm 4** EAF Multi-Resolution (EAF-MR) Algorithm

---

```

1: INPUT: nBit
2:  $\mathbf{x}^{(current)} \leftarrow \mathbf{x}^{(initial)}, \text{SNR}^{(current)} \leftarrow \text{SNR}^{(initial)}, \text{Power}^{(current)} \leftarrow \text{Power}^{(initial)}$ 
3:  $\mathbf{c} \leftarrow \mathbf{c}^{(initial)}$ 
4:  $\mathbf{X} \leftarrow$  a set of configurations obtained by reconfiguring the component  $\mathbf{c}$  with  $n$  bits of control while other components are fixed.
5:  $\text{SNR}^{(cal)}(\mathbf{x}) \leftarrow$  calculated SINR for  $\forall \mathbf{x} \in \mathbf{X}$ 
6:  $\text{Power}(\mathbf{x}) \leftarrow$  power for  $\forall \mathbf{x} \in \mathbf{X}$ 
7:  $\mathbf{x}^{(max)} \leftarrow \arg \max_{\mathbf{x} \in \mathbf{X}} \text{SNR}^{(cal)}(\mathbf{x})$ 
8:  $\mathbf{x}^{(current)} \leftarrow \mathbf{x}^{(max)}$ 
9:  $\text{SNR}^{(current)} \leftarrow$  simulated (or measured) SNR of  $\mathbf{x}^{(current)}$ 
10:  $\text{Power}^{(current)} \leftarrow \text{Power}(\mathbf{x}^{(current)})$ 
11: for  $n = 1, 2, \dots, \text{nBit}$  do
12:    $\mathbf{c} \leftarrow \mathbf{c}^{(initial)}$ 
13:   while (there has been recent updates on  $\mathbf{x}^{(current)}$ ) do
14:      $\mathbf{c} \leftarrow$  the next available component of the current component  $\mathbf{c}$ 
15:      $\mathbf{X} \leftarrow$  a set of configurations obtained by reconfiguring the component  $\mathbf{c}$  with  $n$  bits of control while other components are fixed.
16:      $\mathbf{X}^{(pass)} \leftarrow \{\mathbf{x} \in \mathbf{X} | \text{SNR}^{(cal)}(\mathbf{x}) \geq \text{SNR}_{\text{Threshold}}\}$ 
17:      $\text{SNR}^{(pass)}(\mathbf{x}) \leftarrow$  simulated (or measured) SNR for  $\forall \mathbf{x} \in \mathbf{X}^{(pass)}$ 
18:     if ( $\mathbf{c}$  is a component in a filter) then
19:        $\mathbf{x}^{(max)} \leftarrow \arg \max_{\mathbf{x} \in \mathbf{X}^{(pass)}} \text{SNR}(\mathbf{x})$ 
20:        $\text{SNR}^{(max)} \leftarrow \text{SNR}^{(pass)}(\mathbf{x}^{(max)})$ 
21:       if  $\text{SNR}^{(max)} > \text{SNR}^{(current)}$  then
22:          $\mathbf{x}^{(current)} \leftarrow \mathbf{x}^{(max)}, \text{SNR}^{(current)} \leftarrow \text{SNR}^{(max)}$ 
23:          $\text{Power}^{(current)} \leftarrow \text{Power}(\mathbf{x}^{(current)})$ 
24:       end if
25:     else if ( $\mathbf{c}$  is a component in an amplifier) then
26:       for  $\mathbf{x} \in \mathbf{X}^{(pass)}$  is selected in descending order of  $\text{SNR}^{(pass)}(\mathbf{x})$  do
27:         if  $\text{SNR}^{(pass)}(\mathbf{x}) \geq \text{SNR}_{\text{Spec}} \& \text{Power}(\mathbf{x}) < \text{Power}^{(current)}$  then
28:            $\mathbf{x}^{(current)} \leftarrow \arg \min_{\mathbf{x} \in \mathbf{X}, \text{s.t. } \text{SNR}(\mathbf{x}) \geq \text{SNR}_{\text{Spec}}} \text{Power}(\mathbf{x})$ 
29:            $\text{SNR}^{(current)} \leftarrow \text{SNR}(\mathbf{x}^{(current)})$ 
30:            $\text{Power}^{(current)} \leftarrow \text{Power}(\mathbf{x}^{(current)})$ 
31:         break
32:       end if
33:     end for
34:   end while
35: end for
36: OUTPUT:  $\mathbf{x}^{(current)}, \text{SNR}^{(current)}, \text{Power}^{(current)}$ 

```

---



and  $n\text{Bit}_2$  are the maximal bits of control for reconfiguring components in phase I and phase II, respectively.  $n\text{Bit}_1 = n\text{Bit}_2 = 4$  for our simulation setting. In line 2 to 17, a configuration with maximal simulated SNR (phase I) is found. In line 6, a current component  $\mathbf{c}$  is updated to the next available component. In line 7, a list of configurations to be simulated is obtained by reconfiguring component values at the current component  $\mathbf{c}$  of a current configuration  $\mathbf{x}^{(\text{current})}$ . The resolution for the component reconfiguration is given as  $n$ . In line 9,  $\text{SNR}(\mathbf{x})$  is obtained by simulating configurations of  $\mathbf{x} \in \mathbf{X}$ . In line 18 to 35, a configuration that has the lowest power while meeting a condition  $\text{SNR}(\mathbf{x}) \geq \text{SNR}_{\text{Spec}}$  (Phase II) for  $\mathbf{x} \in \mathbf{X}$  is found.

In Algorithm 4,  $\mathbf{x}^{(\text{current})}$ ,  $\text{SNR}^{(\text{current})}$ ,  $\text{Power}^{(\text{current})}$  represent a current configuration, the simulated SNR and power of the current configuration, respectively. In line 1,  $n\text{Bit}$  is the maximal bits of control for reconfiguring components in phase II, and  $n\text{Bit} = 4$  for our simulation setting. In line 2 to 10, in order to find a configuration with maximal simulated SNR (phase I), calculated SINR is utilized. In line 11 to 36, a configuration that has the lowest power while meeting a condition  $\text{SNR} \geq \text{SNR}_{\text{Spec}}$  (phase II) is found. In line 14, a current component is moved to the next available component and updated to  $\mathbf{c}$ . In line 15, a list of configurations to be simulated is obtained by reconfiguring component values at the current component  $\mathbf{c}$  of a current configuration  $\mathbf{x}^{(\text{current})}$ . The resolution for the component reconfiguration is given as  $n$ .

#### Abbreviations

DARPA: The U.S. Defense Advanced Research Projects Agency; DoD: Department of Defense; DoE: Design of experiments; EAF-MR optimization: Environment-Adaptable Fast Multi-Resolution Optimization; EAF optimization: Environment-Adaptable Fast optimization; FCC: Federal Communications Commission; IF: Intermediate frequency; IIP3: The third-order input intercept point; IP3: The third-order intercept point; LO: Local oscillator; MR optimization: Multi-resolution optimization; MSB: Most significant bit; RF: Radio frequency; RF-FPGA: Radio Frequency-Field Programmable Gate Arrays; SINR: Signal-to-interference-and-noise ratio; SNR: Signal-to-noise-ratio

#### Acknowledgments

This study is sponsored by the DARPA RF-FPGA (Radio Frequency-Field Programmable Gate Arrays) program under Grant HR0011-12-1-0005. The views expressed are those of the authors and do not reflect the official policy or position of the Department of Defense or the U.S. Government.

#### Funding

This study was funded by the DARPA under Grant HR0011-12-1-0005.

#### Availability of data and materials

Not applicable.

#### Authors' contributions

MJ and RN designed the estimation and optimization of the EAF-MR method, demonstrated the method using simulation, and wrote the manuscript. SY contributed to foundational work at the beginning stages of the project. FW, MA, and MS contributed to the implementation of the framework of the circuit specifications and optimization methods for a large-scale RF-FPGA. TM and XL provided advice and insight on the reconfigurable RF-FPGA architecture and optimization. All authors read and approved the final manuscript.

#### Competing interests

The authors declare that they have no competing interests.

#### Publisher's Note

Springer Nature remains neutral with regard to jurisdictional claims in published maps and institutional affiliations.

Received: 8 November 2017 Accepted: 29 January 2018

Published online: 21 March 2018

#### References

1. IF Akyildiz, W-Y Lee, MC Vuran, S Mohanty, Next generation/dynamic spectrum access/cognitive radio wireless networks: a survey. *Comput. Netw.* **50**(13), 2127–2159 (2006)
2. L Anttila, M Valkama, in *Wireless Conference 2011-Sustainable Wireless Technologies (European Wireless), 11th European*. On circularity of receiver front-end signals under RF impairments (VDE, Vienna, 2011), pp. 1–8
3. L Atzori, A Iera, G Morabito, The internet of things: a survey. *Comput. Netw.* **54**(15), 2787–2805 (2010)
4. M Brandolini, P Rossi, D Manstretta, F Svelto, Toward multistandard mobile terminals-fully integrated receivers requirements and architectures. *IEEE Trans. Microw. Theory Tech.* **53**(3), 1026–1038 (2005)
5. DARPA, Radio frequency-field programmable gate arrays (RF-RPGA). (2011). <https://www.fbo.gov/?tab=documents&tabmode=form&subtab=core&tabid=cd49cf41f5df4f860046c3a9bdfef8d9>
6. MS Dayananda, J Priyanka, in *Advanced Communication Control and Computing Technologies (ICACCT), 2012 IEEE International Conference on*. Managing software defined radio through cloud computing (IEEE, Ramanathapuram, 2012), pp. 50–55
7. L Godard, C Moy, J Palicot, in *2006 1st International Conference on Cognitive Radio Oriented Wireless Networks and Communications*. From a configuration management to a cognitive radio management of sdr systems (IEEE, Mykonos Island, 2006), pp. 1–5
8. S Haykin, Cognitive radio: brain-empowered wireless communications. *IEEE J. Sel. Areas Commun.* **23**(2), 201–220 (2005)
9. M Jun, R Negi, J Tao, Y-C Wang, S Yin, T Mukherjee, X Li, L Pileggi, in *2014 IEEE Military Communications Conference*. Environment-adaptable efficient optimization for programming of reconfigurable Radio Frequency (RF) receivers (IEEE, Baltimore, 2014), pp. 1459–1465
10. M Jun, R Negi, Y-C Wang, T Mukherjee, X Li, J Tao, L Pileggi, in *2014 IEEE Globecom Workshops (GC Wkshps)*. Joint invariant estimation of RF impairments for reconfigurable Radio Frequency (RF) front-end (IEEE, Austin, 2014), pp. 954–959
11. M Jun, R Negi, S Yin, F Wang, M Sunny, T Mukherjee, X Li, in *2015 IEEE Global Communications Conference (GLOBECOM)*. Phase noise impairment and environment-adaptable fast (eaf) optimization for programming of reconfigurable Radio Frequency (RF) receivers (IEEE, San Diego, 2015), pp. 1–6
12. LJ Kushner, KW Sliach, GM Flewelling, JD Cali, CM Grens, SE Turner, DS Jansen, JL Wood, GM Madison, in *Radio Frequency Integrated Circuits Symposium (RFIC), 2015 IEEE*. The matrices RF-FPGA in 180nm sige-on-soi bimos (IEEE, Arizona, 2015), pp. 283–286
13. M Lee, M Lucas, R Young, R Howell, P Borodulin, N El-Hinnawy, *Rf fpga for 0.4 to 18 ghz dod multi-function systems. Technical report*. (Northrop Grumman Corp Baltimore MD Electronic Systems, 2013). <http://www.dtic.mil/docs/citations/ADA579506>
14. M Nahas, A Saadani, J-P Charles, Z El-Bazzal, in *Telecommunications (ICT), 2012 19th International Conference on*. Base stations evolution: toward 4G technology (IEEE, Jounieh, 2012), pp. 1–6
15. J Tao, Y-C Wang, M Jun, X Li, R Negi, T Mukherjee, LT Pileggi, in *2014 19th Asia and South Pacific Design Automation Conference (ASP-DAC)*. Toward efficient programming of reconfigurable Radio Frequency (RF) receivers (IEEE, Singapore, 2014), pp. 256–261
16. M Valkama, A Springer, G Hueber, in *Circuits and Systems (ISCAS), Proceedings of 2010 IEEE International Symposium on*. Digital signal processing for reducing the effects of RF imperfections in radio devices—an overview (IEEE, Paris, 2010), pp. 813–816
17. R Zhou, X Li, V Chakravarthy, C Bullmaster, B Wang, R Cooper, Z Wu, in *New Frontiers in Dynamic Spectrum, 2010 IEEE Symposium on*. Software defined radio implementation of smse based overlay cognitive radio (IEEE, Singapore, 2010), pp. 1–2